



Quantifying Patterns and Drivers of Larval Dispersal in Japanese Anchovy (*Engraulis japonicus*) in the China Seas

Wei Shi^{1,2}, Leon Boegman², Shiliang Shan^{2,3}, Yongjun Tian¹, Yang Liu¹, Peng Sun¹, Zhenjiang Ye¹,
Qinwang Xing⁴, Jianchao Li¹

5 ¹Deep Sea and Polar Fisheries Research Center, and Key Laboratory of Mariculture, Ministry of Education, Ocean University
of China, Qingdao, 266100, China

²Environmental Fluid Dynamics Laboratory, Department of Civil Engineering, Queen's University, Kingston, ON K7L 3N6,
Canada

³Department of Physics and Space Science, Royal Military College of Canada, Kingston, ON K7K 7B4, Canada

10 ⁴College of Marine Living Resource Sciences and Management, Shanghai Ocean University, Shanghai, 201306, China

Correspondence to: Jianchao Li (lijianchao@ouc.edu.cn) and Qinwang Xing (qwxing@shou.edu.cn)

Abstract. Larval dispersal is a fundamental process linking marine populations and shaping individual fitness and population connectivity, making its quantification essential for understanding recruitment dynamics in fisheries. However, larval dispersal of the commercially and ecologically important Japanese anchovy (*Engraulis japonicus*), one of the most abundant pelagic
15 fishes in the China Seas, remains poorly understood. Here, we applied 1D and 2D dispersal kernels to quantify larval dispersal outputs from previously published Lagrangian particle-tracking simulations, in which particles were released from seven spawning grounds across the China Seas during April–August (1987–2004 and 2016) and tracked for 30–60 days. We evaluated the relative influences of spawning ground, spawning month and year, and larval travel duration, on dispersal patterns and connectivity. Larval settlement was concentrated in the Bohai Sea, the northern Yellow Sea and along the southern
20 coast of the Shandong Peninsula, with peak densities near 39°N; a Weibull 1D dispersal kernel best described larval dispersal patten, with modal dispersal distances ranges from 44.53 – 150.56 km, identifying these regions as major nursery grounds. Among all factors examined, spawning ground was the dominant driver of dispersal and connectivity, explaining 31.1% of the variance. Larvae from Changjiang Estuary spawning ground dispersed more broadly to the Yellow Sea, Sea of Japan, and the northwestern Pacific, whereas larvae from other grounds were largely retained within the China Seas, highlighting the pivotal
25 role of this ground in linking stocks between these regions. Dispersal patterns exhibited strong seasonal shifts, with enhanced eastward and northward export in spring–early summer and increased retention in late summer. Increasing larval travel duration promoted directional long-range transport while reduced occupied area, local retention, and self-recruitment, indicating that longer dispersal does not imply broader spatial occupation. Pelagic larval duration captured mean dispersal trends but was a poor predictor of individual dispersal outcomes. The relatively minor contribution of interannual variability
30 compared to spatial factors suggests that management should focus more on persistent spatial structures rather than short-term fluctuations. Overall, these findings provide a comprehensive framework for understanding larval dispersal dynamics and offer a robust scientific basis for fisheries management of Japanese anchovy.



35 **1 Introduction**

Understanding and quantifying the patterns and causes of marine larval dispersal is essential for predicting population dynamics and managing marine populations, and has long been a central goal in ecology and conservation biology (Botsford et al., 2001; D'aloia et al., 2015; Sato et al., 2023). Larval dispersal refers to the process by which larvae are transported by currents away from their source populations. Because most marine species experience a pelagic larval phase, larvae may be widely dispersed before recruiting to adult habitats, thereby linking spatially separated populations (Cowen and Sponaugle, 2009; Wood et al., 2013; Faillettaz et al., 2018; Sato et al., 2023). Direct observation of larval dispersal remains challenging due to the small size of eggs and larvae, their potential for long-distance transport, the broad spatial extent of spawning grounds, and a prolonged spawning season (Hao et al., 2003; Zhang et al., 2020b). To overcome these limitations, biophysical models (a hydrodynamic model coupled to a Lagrangian particle tracking model) have been widely applied to investigate larval dispersal in marine fishes (Paris and Cowen, 2004; Zhao et al., 2009; Lett et al., 2010; Chaput et al., 2022).

Despite the applications of these models to Japanese anchovy (*Engraulis japonicus*) (Itoh et al., 2009; Tu et al., 2012; Takeshige et al., 2015; Xing et al., 2020; Xing et al., 2021), however, a comprehensive and quantitative understanding of larval dispersal patterns and their underlying drivers across the China Seas remains lacking. As one of the most abundant pelagic fishes in this region, Japanese anchovy plays a key trophic role and supports both ecological functioning and fisheries production (Zhao et al., 2003). However, its biomass declined sharply from approximately three million tons prior to the mid-1990s to less than 0.5 million tons in the early 2000s, presenting major challenges for fisheries management (Zhao et al., 2003). This collapse has stimulated growing interest in the mechanisms underlying population fluctuations and recruitment dynamics, particularly the role of larval dispersal during early life stages (Tu et al., 2012; Takeshige et al., 2015; Xing et al., 2020; Yu et al., 2020a). While quantifying larval dispersal patterns and their drivers, including spawning location, spawning timing (month and year), and transport duration, can provide critical insights into population connectivity and recruitment processes. Specifically, Xing et al. (2020) and Xing et al. (2021) have applied biophysical models to investigate larval transport of Japanese anchovy, focusing on retention dynamics, larval retention areas (LRAs), and environmental influences on recruitment. However, quantitative analyses of larval dispersal patterns and drivers across China Seas remain lacking.

Dispersal kernel, the probability density function of the dispersal distance from the release location, has been long recognized as a useful framework for quantifying dispersal patterns (Cowen and Sponaugle, 2009; Ayata et al., 2010; Shi et al., 2019; Nathan, 2008; Almany et al., 2017). Because pelagic species often lack clearly defined settlement boundaries, dispersal kernels encompass both successful and unsuccessful dispersal events, avoiding arbitrary definitions of transport success (Huret et al., 2010). However, classical dispersal kernels describe dispersal as a function of distance only and do not capture directionality. These are therefore referred to as a one-dimensional (1D) dispersal distance kernels (Siegel et al., 2003). To address this limitation Edwards et al. (2007) extended the framework to two-dimensional (2D) dispersal location kernels,



enabling the quantification of anisotropic dispersal patterns. Huret et al. (2010) further refined this approach by introducing spatial indices describing occupation, aggregation and dispersion.

Here, we applied both 1D and 2D dispersal kernels to quantify larval dispersal patterns of Japanese anchovy in the China Seas, using particle-tracking outputs from Xing et al. (2020) and Xing et al. (2021). We further performed a multi-factor, multi-
70 variable analysis of variance (MANOVA) to evaluate the impacts of spawning ground, travel duration, spawning year and spawning month on dispersal, and examine the resulting implications for recruitment dynamics and stock connectivity.

2 Materials and Methods

2.1 Study Species and Study Area

In early spring, adult anchovies migrate from their offshore overwintering grounds to coastal waters to spawn (Fig. 1).
75 Spawning occurs from April to October and peaks between May and June (Hao et al., 2003; Zhang et al., 2020b). Embryonic development requires approximately 42–72 hours. Previous studies indicate that anchovy larvae begin to exhibit weak active swimming ability at a body length of 5–7 mm, with swimming capacity gradually increasing between 10 and 20 mm, and reaching a more developed stage at 20–25 mm (Masuda, 2011). Given that the present study focuses on larvae ≤ 20 mm in length (approximately within 30 days post-hatching), active swimming behaviour was neglected following previous
80 approaches, and larvae were treated as passive particles (Takeshige et al., 2015; Xing et al., 2020).

Seven Japanese anchovy spawning grounds (located in the Bohai, Yellow, and East China Seas) were selected for this study (Fig. 1), including: Zhuanghe Bay (ZH; (Ye and Zhang, 1965)); northeast of Bohai Bay and in Laizhou Bay (BHB and LZB, respectively; (Yu et al., 2020b)); Yantai (YT; (Ye and Zhang, 1965)); south of the Shandong Peninsula and in Haizhou Bay (SDI and HZB, respectively; (Zhang et al., 2020b)); and the Changjiang Estuary (CJ; (Iseki and Kiyomoto, 1997)).
85 Lagrangian particles were released and tracked from these sites. Additionally, two spawning grounds for Japanese stocks were included to study connectivity: northwest of Kyushu (TWC; (Takeshige et al., 2015)) and south of Kyushu (PS; (Zenitani and Kimura, 2007)). Notably, no particles were released from these two sites.

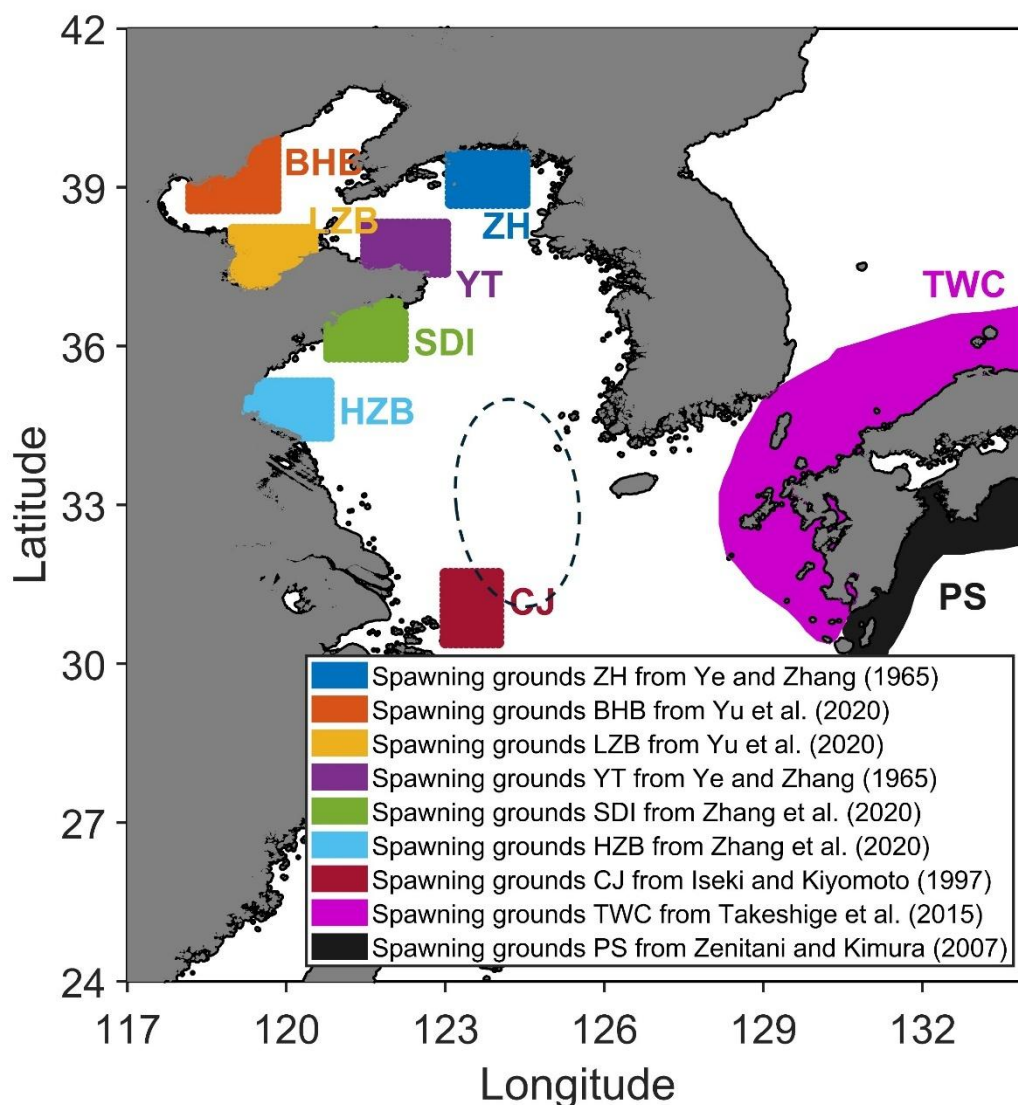


Figure 1. The spawning grounds of Japanese anchovy (*Engraulis japonicus*) in the China Sea, Japan Sea and Pacific Ocean, which also represent the larval particle release locations used in the particle tracking models (with the exception of TWC and PS). The areas are: Zhuanghe Bay (ZH; (Ye and Zhang, 1965)); northeast of Bohai Bay and Laizhou Bay (BHB and LZB, respectively; (Yu et al., 2020b)); Yantai (YT; (Ye and Zhang, 1965)); south of the Shandong Peninsula and in Haizhou Bay (SDI and HZB, respectively; (Zhang et al., 2020b)); the Changjiang Estuary (CJ; (Iseki and Kiyomoto, 1997)); northwest of Kyushu (TWC; (Takeshige et al., 2015)); and south of Kyushu (PS; (Zenitani and Kimura, 2007)). The white area represents the ocean and grey represents land. The dashed ellipse represents the overwintering ground (Zhao, 2006).



2.2 Hydrodynamic and Lagrangian Particle Tracking Model

Lagrangian particle tracking simulations from Xing et al. (2020) and Xing et al. (2021), which investigated larval retention of Japanese anchovy in 2016 and over the period 1987–2004, were applied in this study. The hydrodynamic modal and Lagrangian particle tracking model were described as follows.

100 The Finite Volume Coastal Ocean Model (FVCOM) was used to simulate the hydrodynamic fields for larval dispersal. This model has been successfully applied to study larval retention of Japanese anchovy in the Yellow Sea (Xing et al., 2020; Xing et al., 2021). The model configuration features a horizontal resolution of 6.5 km (41 sigma layers vertically), with a mesh of 44,682 nodes and 86,107 grids. The time step was 40 s and hourly current data from 1987 to 2018 were generated by the model and used for particle tracking. Over 4 months in 2012 and 2013 the model reproduced subtidal current velocities with
105 root-mean-square errors of 0.70 to 3.24 cm/s. Further details on model configuration and validation are available in Xing et al. (2020).

Given the weak swimming ability of Japanese anchovy below 20 mm in length, a 2D Lagrangian particle tracking model was developed to simulate the passive transport of fish larvae, with active swimming behavior neglected (Takeshige et al., 2015; Xing et al., 2020). In this algorithm, a fourth-order Runge-Kutta scheme was used to prevent excessively large truncation
110 errors. Random walk was also considered to resolve sub-grid scale phenomenon, such as horizontal turbulent flow (Willis, 2011; Choi et al., 2018). The horizontal diffusivity coefficient was based on the Smagorinsky diffusivity scheme (Choi et al., 2018). The time step for this particle tracking model was set as 1 h. The hydrodynamic fields from the FVCOM simulation served as the driver for the particle movements. A comprehensive description of the algorithm is provided by Xing et al. (2020). Larval release was specified as follows.

115 **Larval release location:** Larval particles were released from the seven spawning grounds identified in China Seas in Fig. 1 (ZH, BHB, LZB, YT, SDI, HZB, CJ). Each site was divided into ~ 150 grid cells, consistent with the FVCOM grid. All particles were released from the center of the grid; and they were released in the surface layer as living eggs and larvae for Japanese Anchovy have typically been found near the surface (Iseki and Kiyomoto, 1997). Larval vertical migration and larval mortality were not considered in this study.

120 **Larval release time:** To study the effects of spawning month and year on larval dispersal, particles were released annually on the 1st, 11th, and 21st of each month from April to August during 1987 – 2004 (Xing et al., 2021) and also in 2016 (Xing et al., 2020). This resulted in 15 releases per year (3 times per month × 5 months), totaling 285 release events over the 19-year period (15 times per year × 19 years).

Larval tracking duration: The pelagic larval duration (PLD) ranges from 30 to 60 days (Takeshige et al., 2015; Huggett
125 et al., 2003; Lett et al., 2006; Xing et al., 2020; Xing et al., 2021; Lett et al., 2007). Accordingly, larval tracking was conducted with durations of 30, 40, 50, 60 days, respectively.

Larval release number: A total of 1197000 particles (7 spawning grounds × 150 grid cells per site × 19 years × 15 days per year × 4 durations = 1197000 particles) were released in this simulation.



Larval settlement location: The position of a particle at the end of its PLD is referred to as its settlement location.

130 2.3 1D Dispersal Distance Kernel

The 1D dispersal kernel has been long recognized as a useful approach to quantify dispersal patterns of plant seeds, insects and fish larvae (Cowen and Sponaugle, 2009; Ayata et al., 2010; D'aloia et al., 2015; Almany et al., 2017; Shi et al., 2019; Shi et al., 2024). It represents the probability density function (PDF) of these dispersal distances, which is defined as the straight-line distance between a particle release location and its settlement location. In this study, dispersal distances from all 19
135 simulated years were aggregated for each spawning ground to compute a unique kernel for each ground. Additionally, a separate, combined kernel was calculated by pooling dispersal distances from all grounds, resulting in a total of eight dispersal kernels (seven for the individual grounds and one collective kernel).

The kernel can provide three important metrics characterizing larval dispersal: local retention, mean- (or median-) dispersal distance, and long-distance dispersal (Nickols et al., 2015). Local retention is the ratio of locally produced settlement to total local larval release, determining the self-persistence of a population (Botsford et al., 2009). The median-dispersal
140 distance describes the distance within which half of larvae settle. Long-distance dispersal, usually defined as the 95th-percentile dispersal distance, is important for estimating population invasion, population spread, and genetic connectivity (Cowen and Sponaugle, 2009; Nathan, 2008; Nathan et al., 2008). Self-recruitment, which is related to but distinct from local retention (Botsford et al., 2009), was also computed. It represents the ratio of locally produced settlement to settlement from all origins
145 at a site.

2.4 2D Dispersal Location Kernel

The kernel above is a function of distance only, and does not convey information on direction. It is thus referred to as a 'one-dimensional (1D) dispersal distance kernel' (Siegel et al., 2003). Edwards et al. (2007) extended the 1D kernel into two dimensions (2D), as a '2D dispersal location kernel', by computing a set of indices to describe the kernel in areas with strong
150 anisotropy in circulation. Huret et al. (2010) further refined this approach by introducing spatial indices related to spatial occupation and aggregation. Several indices were defined to characterize the 2D larval dispersal location kernels, enabling statistical analysis of the particle distributions (Edwards et al., 2007; Ayata et al., 2010; Hinrichsen et al., 2012; Puckett et al., 2014).

(i) The geographic position of the settlement locations, included the center of gravity, x_m , y_m , along with the associated
155 variances and covariance, S_x , S_y , and S_{xy} .

(ii) The mean relative transport, included the mean orthodromic distance and direction from release center (x_0, y_0) to settlement center (x_m, y_m) , i.e., d_m and θ . Here, θ represents the direction measured clockwise from north.

$$d_m = R_e \operatorname{acos} \left[\sin \frac{\pi y_m}{180} \sin \frac{\pi y_0}{180} + \cos \frac{\pi y_m}{180} \cos \frac{\pi y_0}{180} \cos \left(\frac{\pi x_0}{180} - \frac{\pi x_m}{180} \right) \right]$$



$$\theta = \arctan2\left(\sin\left(\frac{\pi x_m}{180} - \frac{\pi x_0}{180}\right) \cos\left(\frac{\pi y_m}{180}\right), \cos\left(\frac{\pi y_0}{180}\right) \sin\left(\frac{\pi y_m}{180}\right) - \sin\left(\frac{\pi y_0}{180}\right) \cos\left(\frac{\pi y_m}{180}\right) \cos\left(\frac{\pi x_m}{180} - \frac{\pi x_0}{180}\right)\right) \times \frac{180}{\pi}$$

160 (iii) The dispersion or variance around the center of gravity is the inertia (I). It is the mean square distance between an individual fish and the center of gravity of the population (Woillez et al., 2009). It is not identical in every spatial direction, and can be decomposed into two principal orthogonal axes, which represent the maximum ($amaj$) and the minimum ($amin$) components overall inertia. A principal component analysis (PCA) of particle positions provides these axes, which can be visualized in space as an ellipse. The ellipse characteristics include the length of the major axis ($amaj$), its orientation (θ_m),
 165 the length of the minor axis ($amin$), and the isotropy (iso).

$$I = \frac{1}{n} \sum_{i=1}^n ((x_i - x_m)^2 + (y_i - y_m)^2)$$

$$amaj = \sqrt{\frac{1}{2} \left(S_x + S_y + \sqrt{(S_x - S_y)^2 + 4S_{xy}^2} \right)}$$

$$amin = \sqrt{\frac{1}{2} \left(S_x + S_y - \sqrt{(S_x - S_y)^2 + 4S_{xy}^2} \right)}$$

$$\theta_m = \frac{180}{\pi} \cdot \frac{1}{2} \arctan2(2S_{xy}, S_x - S_y)$$

170

$$iso = \frac{amin}{amaj}$$

(iv) For a given inertia, the spatial distribution of particles can exhibit a range of patterns at smaller scales, depending on how space is occupied, from a homogeneous density distribution to pronounced aggregations. To characterize these spatial patterns, we used indices developed by Woillez et al. (2009) for analyzing adult fish populations: positive area (PA), spreading area (SA), equivalent area (EA), and the coefficient of variation of positive values of densities (CV_0). PA is defined as the sum
 175 of area units containing at least one particle, calculated as the number of grids with at least one particle multiplied by the area of each grid (S). SA quantifies how densities are distributed within the PA , as follows:

$$SA = 2 \int \frac{(Q - Q(A))}{Q} dA$$

where A is the cumulated area occupied by the density values, ranked in decreasing order. $Q(A)$ is the corresponding cumulated abundance and Q is the total abundance. EA measures the inverse probability that two randomly chosen particles
 180 settled in the same grid cell. It is defined as:

$$EA = \frac{S \times (\sum_i d_i)^2}{\sum_i d_i^2}$$

where d_i is the particle density in cell i of the model domain. Finally, CV_0 is defined as:



$$CV_0^2 = \frac{PA}{EA} - 1$$

2.5 Connectivity Matrix

185 The connectivity matrix is structured with spawning locations (sources) on the y-axis and settlement locations (sinks) on the x-axis. Each element of the matrix, $C_{i,j}$, represents the proportion of fish larvae transitioning from source i to sink j and is computed as the number of particles transported from i to j ($N_{i,j}$) divided by the number of particles released from i (N_i). In this study, all nine spawning grounds (including both Chinese and Japanese sites) were designated as potential sinks to investigate their connectivity. A seasonal connectivity matrix was constructed for each month from April to August. The values
190 in the TWC and PS rows are undefined, as no larvae were released from these two grounds in the present study; however, dispersal from the Chinese grounds to the Japanese sites can occur.

The diagonal elements of each matrix, $C_{i,i} = N_{i,i}/N_i$, represent local retention (Fig. 5), defined as the ratio of locally produced settlers to total locally released larvae (Botsford et al., 2009). Self-recruitment can be computed as $N_{i,i}/\sum_j N_{j,i}$ (Gamoyo et al., 2019; Paris et al., 2007; Paris et al., 2013; Sponaugle et al., 2012). Notably, this measure reflects the relative
195 variability in self-recruitment rather than its absolute value, as the realistic value of self-recruitment depends on the number of particles released from the spawning ground in forward-in-time particle tracking simulations (Shi et al., 2026a).

2.6 Statistical Analysis

We performed a multi-factor, multi-variable analysis of variance (MANOVA) to evaluate the impacts of spawning ground, travel duration, spawning year and spawning month on dispersal. The factors included spawning ground, travel duration,
200 spawning year and spawning month. Variables comprised seven metrics : (i) the geographic position of the center of gravity ($x_m, y_m, S_x, S_y,$ and S_{xy}), (ii) the mean relative transport indices (mean distance and direction of the center of gravity from the release location, d_m and θ), (iii) the ellipse characteristics ($I, amaj, amin, iso,$ and θ_m), (iv) spatial and aggregation indices (PA, SA, EA and CV_0), (v) connectivity between each spawning ground ($\sum_i C_{i,ZH}, \sum_i C_{i,BHB}, \sum_i C_{i,LLZB}, \sum_i C_{i,YT}, \sum_i C_{i,SDI}, \sum_i C_{i,HZB}, \sum_i C_{i,CJ}, \sum_i C_{i,TWC}, \sum_i C_{i,PS}$), (vi) local retention, and (vii) self-recruitment. The MANOVA was performed
205 using the 50-50 MANOVA Matlab® code from Langsrud (2002), which is designed to handle multiple highly collinear response variables.

3 Results

3.1 Dispersal Patterns

Japanese anchovy larvae were simulated to settle over a wide range, while were concentrated in the Bohai Sea, the northern
210 Yellow Sea and along the southern coast of the Shandong Peninsula, with peak densities near 39°N, identifying these regions

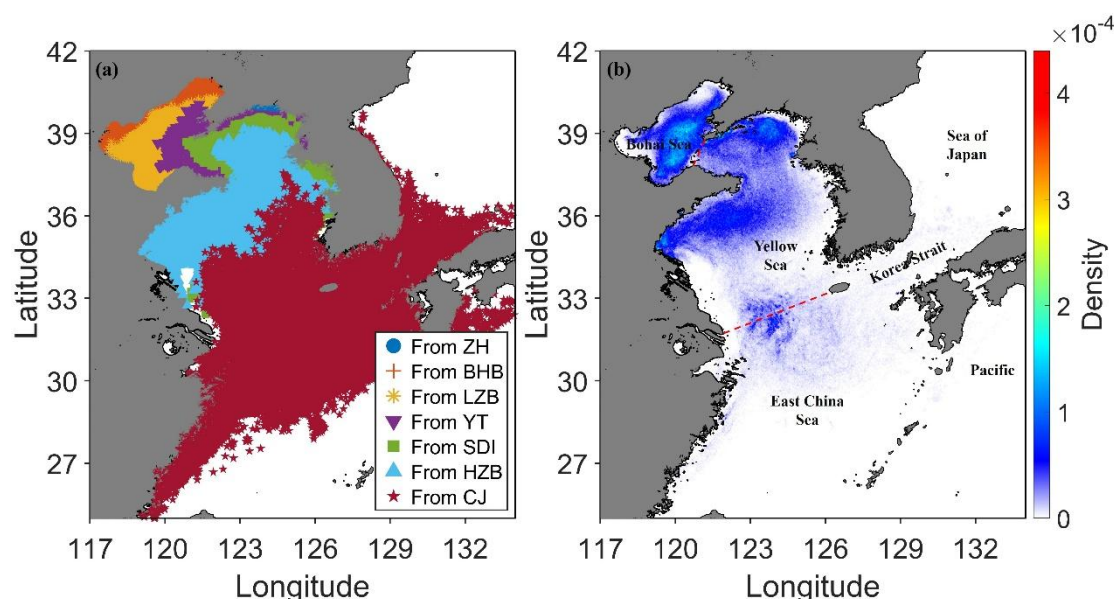


as major nursery grounds. From 1987 – 2004 and in 2016, larvae dispersed widely during their pelagic stage, encompassing the Bohai, Yellow, and East China seas, the Korea Strait, the Sea of Japan, and the northwestern Pacific (Fig. 2). Settlement density gradually decreased southward and offshore (except in the Bohai Sea), consistent with a predominantly northward transport pattern driven by regional circulation (Xing et al., 2020).

215 We estimated the 1D dispersal kernel by fitting various PDFs to the modelled dispersal distances. The best-fitting 1D dispersal kernel was a Weibull function (Table S1 from supporting information; Fig. 3):

$$\rho(d) = \frac{a}{\lambda} \left(\frac{d}{\lambda}\right)^{a-1} \cdot e^{-(d/\lambda)^a}$$

where $\rho(d)$ is the probability density function, d is the dispersal distance (in kilometers). The scale parameter is $\lambda=164.31$, and the shape parameter is $a=1.48$. The modal dispersal distance was 73.31 km, the median-dispersal distance was 128.37 km, 220 and the long-distance dispersal threshold was 344.03 km.



225 **Figure 2.** (a) Larval settlement patterns of Japanese anchovy (*Engraulis japonicus*) by spawning ground. White areas represent the ocean, grey areas represent land, and each color corresponds to settlement locations originating from a specific spawning ground. (b) Density distribution of all settled larvae, calculated as the number of larvae settled in each cell divided by the total number of larvae.

3.2 Variation in Dispersal



3.2.1 Quantifying Effects on the Dispersal and Connectivity

MANOVA revealed that all factors (spawning ground, travel duration, spawning year and spawning month), and most of their interactions, significantly affected the metrics (p -value were < 0.05 in most cases; Table 1), while spawning ground was the most influential, and spawning year was the least influential. Specifically, spawning ground explained the greatest amount of variance (31.1%) in the dispersal kernel and connectivity. It also accounted for the highest proportion of variance within each set of indices: geographic position (44.6%), connectivity (33.1%), self-recruitment (31.8%), relative position (29.6%), local retention (26.4%), ellipse (25.1%), and aggregation (18.5%). In contrast, spawning year explained the smallest proportion of variance across indices, including relative position (2.3%), ellipse (1.1%), aggregation (1.5%), local retention (1.3%), self-recruitment (1.2%), and had the lowest overall effect on the combined indices (1.2%). Spawning month contributed the second-highest proportion of variance for most set of indices, for instance, 3.5% for geographic position, 6.9% for relative position, 2.2% for connectivity, 7.8% for local retention, and 4.9% for self-recruitment.

Table 1. Results of a MANOVA performed on six sets of response variables: (i) the geographic position of the center of gravity for settled particles, (ii) the relative position of the center of gravity (i.e., the distance and direction from the release locations' center of gravity to the settlement locations' center of gravity), (iii) parameters of the variance of the distribution (ellipse), (iv) parameters related to space occupation and aggregation, (v) connectivity between each spawning grounds, (vi) local retention (LR), (vii) self-recruitment (SR), and (viii) the whole set of parameters (all). Values are percentages, representing the proportion of variance in one set of response variable that is explained by each factor. An asterisk (*) denotes non-significant effects ($p > 0.05$).

Factor	d.f.	Geographic position	Relative position	Ellipse	Aggregation	Connectivity	LR	SR	All
Spawning ground (G)	6	44.6	29.6	25.1	18.5	33.1	26.4	31.8	31.1
Travel duration (D)	3	2.0	3.5	3.5	6.6	0.4	4.4	4.3	2.7
Year (Y)	18	1.0	2.3	1.1	1.5	0.9	1.3	1.2	1.2
Month (M)	4	3.5	6.9	2.8	1.9	2.2	7.8	4.9	3.2
G × D	18	2.2	1.1	1.8	1.7	3.0	0.9	1.6	2.2
G × Y	108	4.6	5.8	7.3	8.4	5.6	7.6	5.7	6.3
G × M	24	8.9	9.9	8.5	13.0	11.7	20.5	7.0	10.9
D × Y	54	0.2	0.2*	0.2*	0.4	0.3	0.1*	0.2*	0.2
D × M	12	0.4	0.4	0.2	0.3	0.3	1.0	0.6	0.3
Y × M	72	1.8	3.8	2.6	4.0	1.9	2.2	2.0	2.5
G × D × Y	324	0.9*	0.9*	1.5*	1.2*	1.7	0.4*	1.5	1.3



$G \times D \times M$	72	1.9	1.2	1.0	1.7	2.5	1.2	2.1	1.8
$G \times Y \times M$	432	9.4	10.4	14.3	15.1	12.2	10.9	10.1	12.2
$D \times Y \times M$	216	0.6	0.9*	0.9*	0.9*	1.0	0.4*	0.9*	0.9
$G \times D \times Y \times M$	1296	3.4*	3.4*	4.8*	3.9*	6.6	2.6*	5.5	4.8
Residuals	5320	14.7	19.9	24.2	20.9	16.5	12.3	20.5	18.4

3.2.2 Spatial Variability of Dispersal

Since the spawning ground contributed most to the variance in larval dispersal, the spatial variability of the dispersal patterns was presented (Fig. 2a and Fig. S1), 1D and 2D dispersal kernels were computed (Fig. 3a, 3b and 4).

250 Settlement locations differed significantly between the spawning grounds: larvae from BHB and LZB (located in the Bohai Sea) settled primarily within the Bohai Sea; larvae from ZH, YT, SDI, and HZB (located in the Yellow Sea) settled in the Yellow Sea; whereas larvae from CJ dispersed more broadly, reaching the Yellow Sea, the Sea of Japan and the northwestern Pacific (Fig. S1). From 1987 – 2004 and in 2016, all Japanese anchovy larvae from ZH, BHB, LZB, and YT settled exclusively in the Bohai and Yellow Seas, with none reaching the East China Sea, Sea of Japan and Pacific (Fig. S1).
 255 Most larvae from SDI and HZB also settled in the Bohai and Yellow Seas, though a few reached the East China Sea (~1.5%-3%) and the Jeju Strait (<2%). Notably, none from these northern grounds (ZH, BHB, LZB, YT, SDI, and HZB) settled in the Tsushima Strait or near Kyushu, underscoring the Bohai and Yellow Seas as key nursery areas. In contrast, larvae from CJ dispersed more widely, settling in the Yellow Sea, East China Sea, Korea Strait (comprising the Jeju and Tsushima Straits), and waters off Kyushu (Fig. 2a). Many reached Japanese nursery grounds, highlighting the crucial role of CJ in larval exchange
 260 between Chinese and Japanese anchovy stocks. This is shown by zero-dispersal from the other more northern grounds, but relatively high dispersal from CJ to TWC and PS regions (Fig. 4).

Dispersal kernels varied markedly among spawning grounds, with CJ exhibiting dispersal distance approximately twice those of LZB. Larvae from CJ, compared to from other grounds, exhibited the second largest modal dispersal distance (131 km), the largest median-dispersal distance (196 km) and the greatest long-distance dispersal threshold (495 km). This indicates
 265 that larvae originating from CJ settled at greater distances overall, with 50% of individuals dispersing farther than 196 km and 5% dispersing farther than 495 km. The CJ ground provided greater opportunities for larval transport over long distances and into the Sea of Japan and northwestern Pacific. In contrast, larvae from LZB exhibited the second smallest modal dispersal distance (48 km), the smallest median-dispersal distance (73 km), and the smallest long-distance dispersal threshold (186 km). For larvae released from ZH, BHB, LZB, YT, SDI, HZB, and CJ, the modal dispersal distances were 45 to 150 km (Figure
 270 3a); the median-dispersal distances were 73 to 196 km (Figure 3b); the long-distance dispersal thresholds were 186 to 495 km, respectively (Figure 3b). The modal dispersal distances were considered to be the most important nursery region, as the frequency of larval settlement was highest within this range. The PDF kernels became progressively flatter for LZB, BHB, ZH, HZB, YT, SDI, and CJ, with corresponding kurtosis of 4.2 to 13.2 (Fig. 3a).



Several sets of indices varied significantly between the spawning grounds (Fig. 4). Larvae from CJ exhibited the greatest
275 mean orthodromic distance (d_m), the largest dispersion around their centre of gravity (Inertia), the highest spatial heterogeneity
in density (CV_θ), and the highest dispersal rate to the TWC and PS regions, yet one of the smallest local retention (LR) values.
Notably, despite their longer dispersal, they exhibited one of the smallest PA, SA, or EA. This suggests that, although they
travelled farther, their dispersal was strongly directional and spatially aggregated, resulting in lower PA, as reflected by the
high spatial heterogeneity in density (CV_θ). In contrast, larvae from LZB exhibited the shortest d_m , with the highest LR and
280 SR.

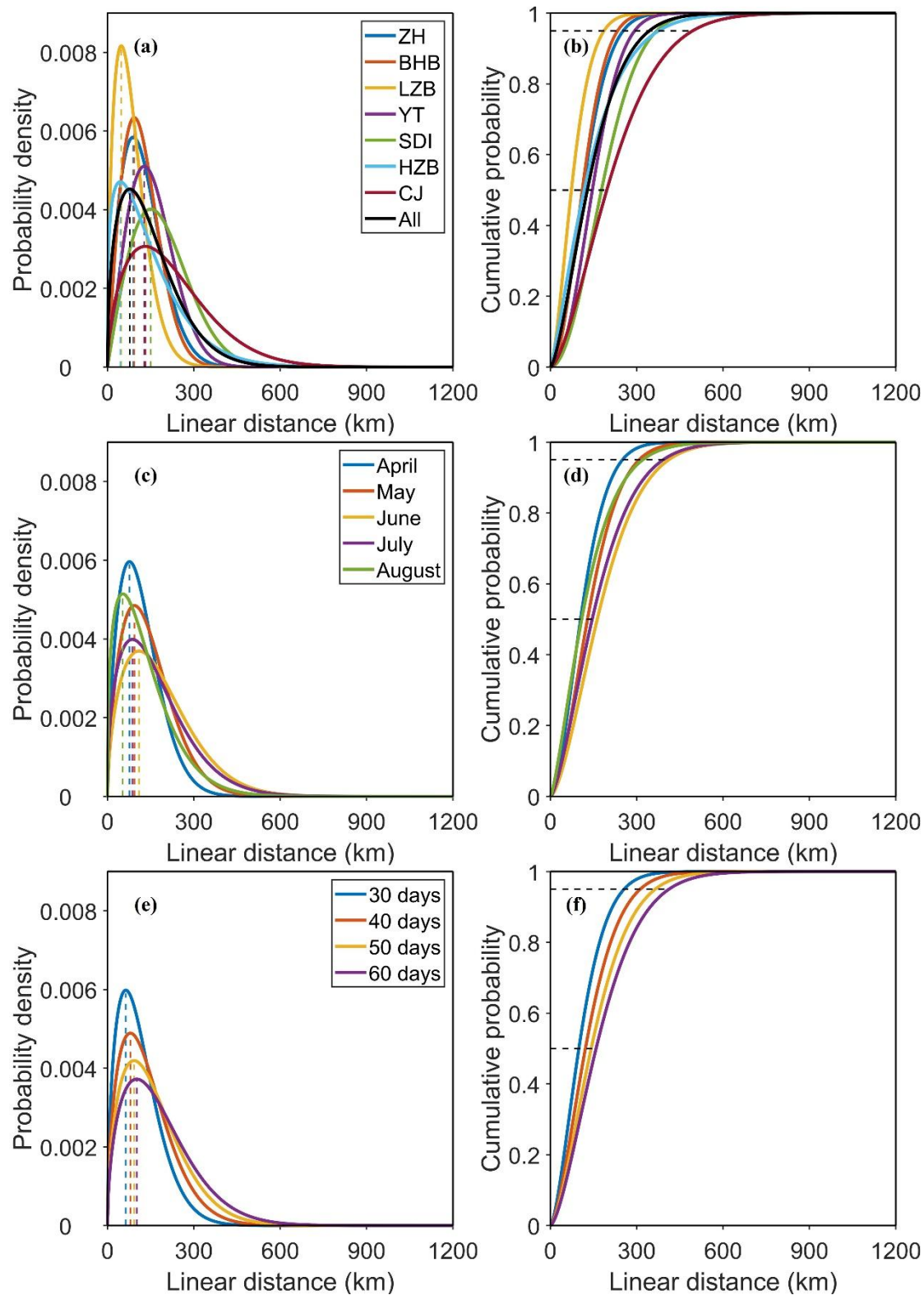


Figure 3. Dispersal kernel, the probability density function (PDF) of dispersal distances between spawning grounds and settlement locations, for Japanese anchovy (*Engraulis japonicus*) larvae, by (a) spawning ground, (c) spawning month, and (e) travel duration. (b) Cumulative distribution function (CDF) of dispersal distances, by (b) spawning ground, (d) spawning month, and (f) travel duration. Dashed lines in the left panel represent modal dispersal distances. Dashed lines in the right panel at $y = 0.5$ and $y = 0.95$ represent median-dispersal distance and long-distance dispersal, respectively.

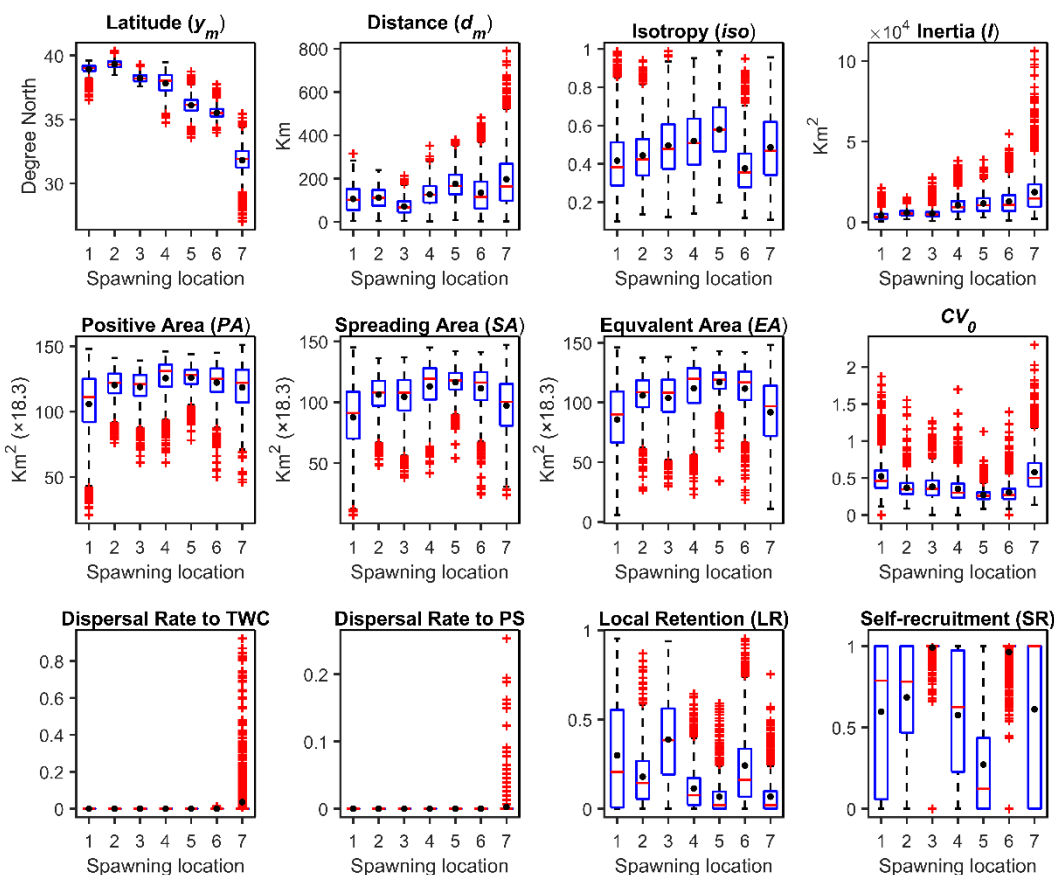


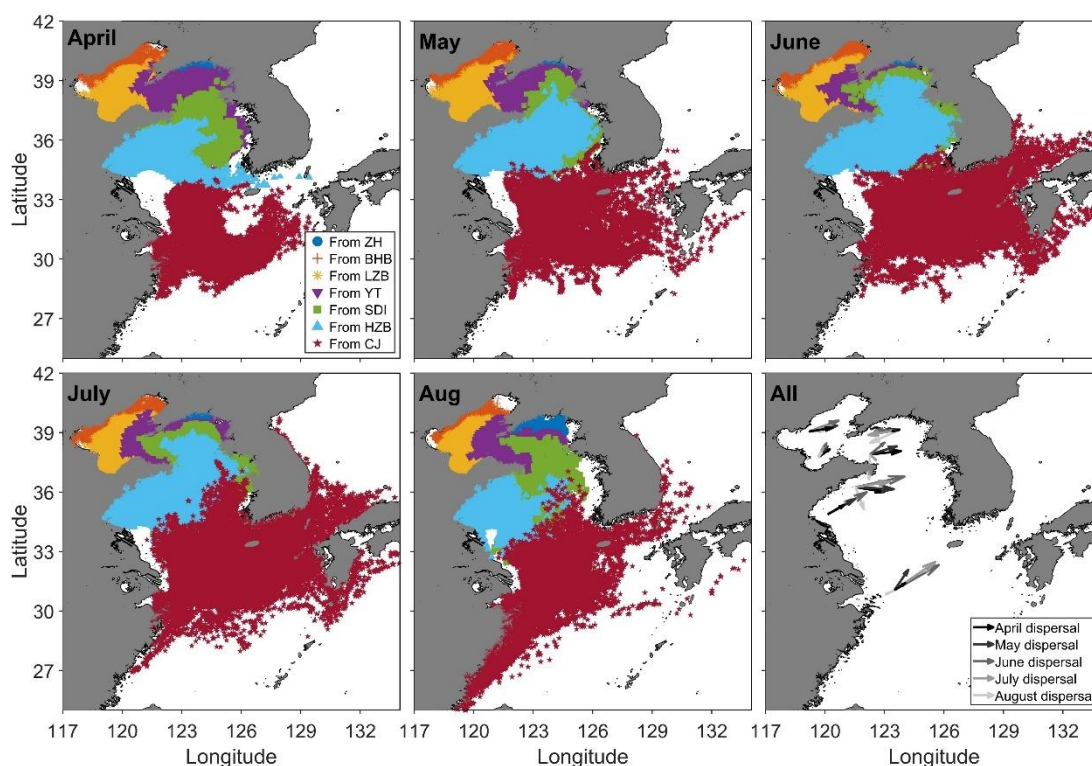
Figure 4. Box plots and means of selected indices describing the dispersal of Japanese anchovy (*Engraulis japonicus*) from seven discrete spawning locations. Extreme values, defined as outliers, are represented by dots. Statistics were computed from the 4 travel durations and 15 release dates per year over the periods 1987-2004 and 2016. Locations 1 to 7 correspond to the spawning locations ZH, BHB, LZB, YT, SDI, HZB, and CJ, respectively.

3.2.3 Seasonal Variability of the Dispersal

The spawning month accounted for the second-highest proportion of variance in geographic position, relative position, and ellipse indices. The settlement location distributions (Fig. 5), 1D dispersal kernel (Fig. 3c and d) and 2D dispersal kernel metrics (Fig. 6) by spawning month were thus presented.



A clear seasonal shift in dispersal was observed: most larvae moved eastward and northward from April to June, but shifted westward and southward since July (Fig. 5); correspondingly, local retention declined initially and increased since July (Fig. 6). The center of gravity of settlement was predominantly located east of the release locations for most groups, except for the ZH group, which exhibited a westward displacement (Fig. 5, bottom right panel). Interestingly, the settlement center of gravity shifted eastward and northward from April to June, but shifted westward and southward since July (Fig. 5, bottom right panel). The modal dispersal distance, median dispersal distance, and long-distance dispersal threshold from 1D dispersal kernel, increased from April to June and decreased from July to August (Fig. 3c and d). The d_m , I , and dispersal rate to TWC from the 2D dispersal kernel, increased from April to June and decreased from July to August, whereas LR and SR showed the opposite trend (Fig. 6).



305

Figure 5. Larval settlement patterns of Japanese anchovy (*Engraulis japonicus*) by spawning ground and month. The white area represents the ocean, grey represents land, and each color corresponds to settlement locations from a specific spawning ground. Arrows in the bottom right panel indicate the mean larval dispersal from the release center to the settlement center. The arrow color turns from black to light grey as the season progresses and indicates the mean distance and direction from the center of gravity of release locations to the center of gravity of settlement locations.

310

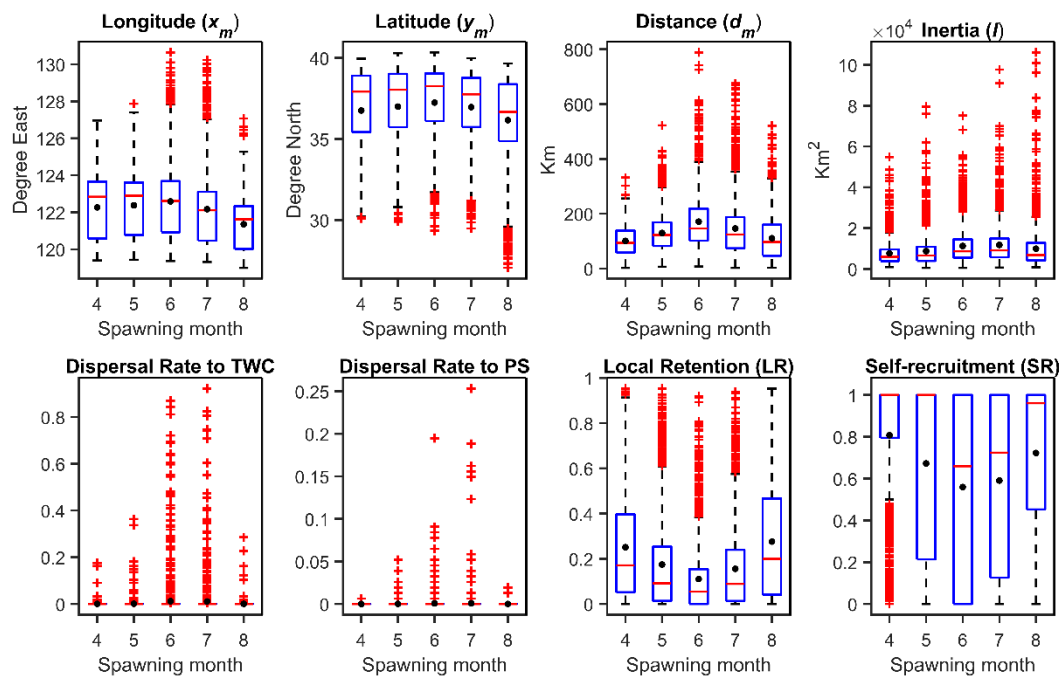
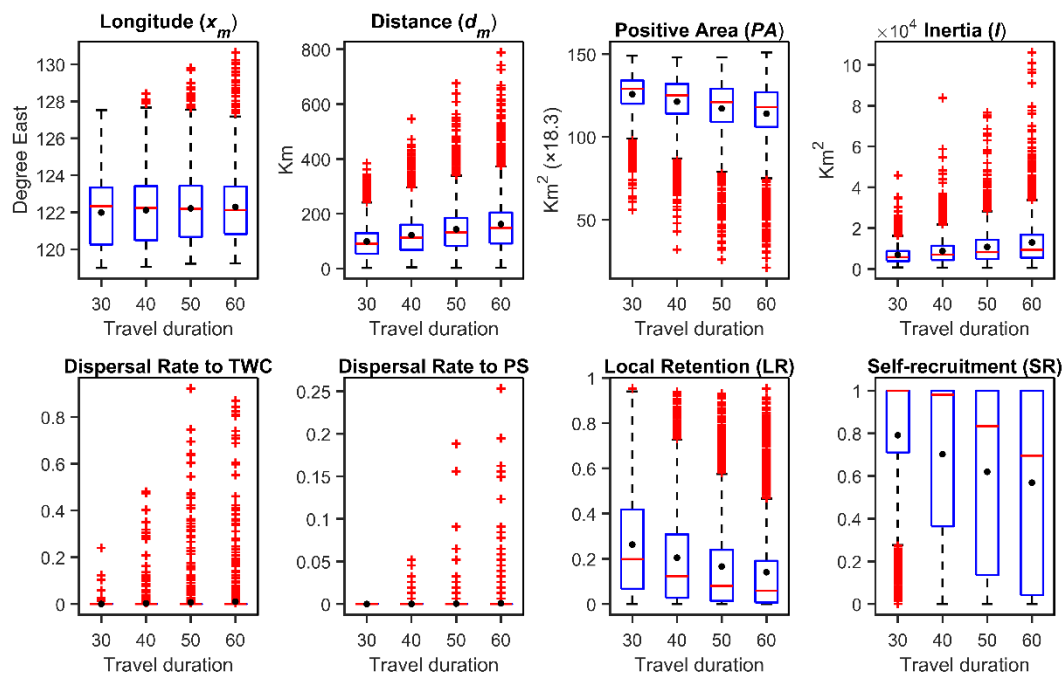


Figure 6. Box plots and means of selected indices describing the dispersal of Japanese anchovy (*Engraulis japonicus*) from April (month 4) through August (month 8). Extreme values, defined as outliers, are represented by red pluses. Statistics were computed from the 4 travel durations and 7 spawning locations per year over the periods 1987-2004 and 2016.

3.2.4 Impact of Larval Travel Duration on Dispersal

Mean orthodromic distance from release centre to settlement centre (d_m) increased with travel duration, while PA (the sum of area units containing at least one particle) decreased, indicating that a longer dispersal distance does not necessarily correspond to a broader dispersal region. The 1D dispersal kernels (PDF) became progressively flatter from 30 days to 60 days, while modal dispersal distance, median dispersal distance, and long-distance dispersal threshold all increased from 30 days to 60 days (Fig. 3 e and f). Several indices related to the 2D kernel varied approximately linearly with increasing travel duration (Fig. 7): the longitude of settlement centre (x_m) shifted eastward by 0.01° , d_m increased by 2.1 km, PA decreased by $0.4 \times 18.3 \text{ km}^2$, inertia (I) increased by 202 km^2 , local retention (LR) decreased by 0.004 and self-recruitment (SR) decreased by 0.008, per 10 days.



325

Figure 7. Box plots and means of selected indices describing the dispersal of Japanese anchovy (*Engraulis japonicus*) in 4 travel durations. Extreme values, defined as outliers, are represented by dots. Statistics were computed from the 7 spawning locations and 15 release dates per year over the periods 1987-2004 and 2016.

3.3 Consequences of Dispersal

330 Connectivity varied significantly between locations. For example, LZB exhibited strong self-connectivity (local retention) but showed almost no connectivity to other regions (Fig. 8). Spawning month accounted the second-highest proportion of variance for connectivity, its effects on connectivity are thus presented in Fig. 8. Travel duration had the weakest effect on connectivity (MANOVA; Table 1). Connectivity displayed clear seasonal patterns. Excluding the TWC and PS regions (where no particles were released), the colored cells in the inner matrices were predominantly concentrated above the diagonal in April. These

335 cells gradually became lighter from April to August, whereas those below the diagonal became progressively darker during the same period. This pattern shows that larvae were primarily transported eastward and northward in April but moved in the opposite direction by August. In addition, only larvae from CJ ground reached TWC and PS regions.

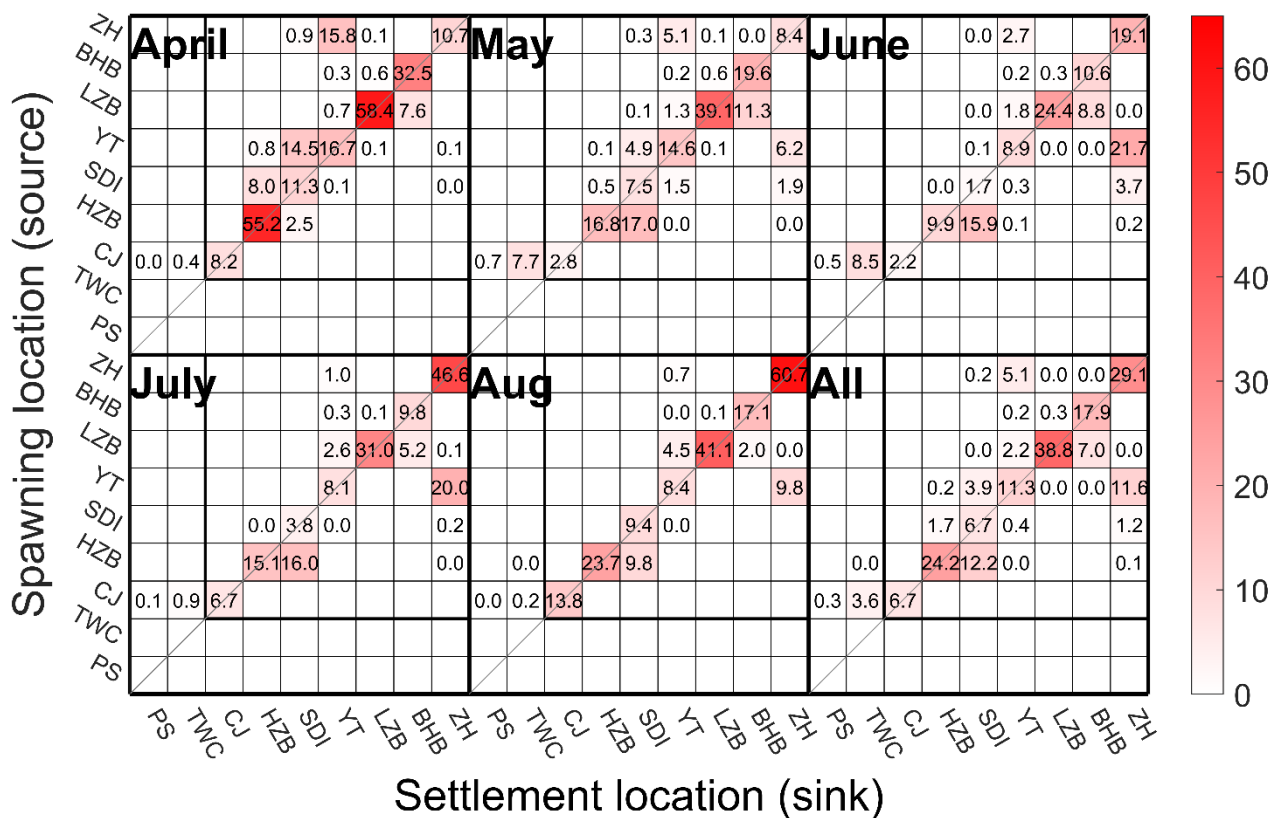


Figure 8. Multi-month connectivity matrices presenting the proportion (%) of Japanese anchovy (*Engraulis japonicus*) larvae transitioning from spawning locations/sources (y-axis) to settlement locations/sink (x-axis). Local retention within each area is represented on the diagonal. Blank cells indicate no connectivity, whereas cells with a value of 0.0 denote extremely low connectivity, approaching zero.

4 Discussion

4.1 Dominant Role of Spawning Ground in Larval Dispersal of Japanese Anchovy

Spawning grounds played a critical role in shaping larval dispersal patterns in this study, as they were distributed across three distinct marine systems, the Bohai Sea, Yellow Sea, and East China Sea (spanning approximately 8° of latitude), each characterized by different prevailing current regimes. For example, the CJ spawning ground, located in the East China Sea, is strongly influenced by the Changjiang Diluted Water (Xing et al., 2020), which promotes eastward transport. In contrast, the BHB and LZB spawning grounds, located in the Bohai Sea, are primarily governed by basin-scale circulation and coastal currents (Liang and Sun, 2003), resulting in relatively constrained dispersal and higher local retention. These differences in regional hydrodynamics among spawning grounds fundamentally influence larval transport pathways, dispersal distances, and



connectivity patterns. By contrast, the contributions of other variables (e.g., travel duration, spawning month and year) were relative minor.

355 However, the relative importance of these factors varies across environments and species. For instance, Huret et al. (2010) applied a particle tracking approach to investigate larval dispersal patterns of *Engraulis encrasicolus* in the Bay of Biscay and applied MANOVA to evaluate impacts of the various factors on 2D dispersal kernel metrics, including release date, spawning date (week and year), spawning ground (five grounds spanning 3.5° of latitude), travel duration, and vertical behavior. Their results showed that spawning location explained most of the variance in geographic and relative positions, travel duration dominated the variance in ellipse, and vertical behaviour primarily influenced aggregation patterns.

360 4.2 Pelagic Larval Duration as a Proxy for Dispersal Distance

Previous studies have reported conflicting results on using PLD as a proxy for dispersal distance; here we show that while it reasonably approximates mean dispersal, it poorly predicts the realized dispersal of individual larvae. Shanks et al. (2003) and Shanks (2009) compiled independent, direct estimates of dispersal distance and compared them to propagule duration (a broader term encompassing PLD). Both studies found that, at a coarse scale, propagule duration was moderately correlated 365 ($R^2=0.6$) with dispersal distance. Selkoe and Toonen (2011) further demonstrated a consistent, moderate fit between genetic proxies of dispersal (using either isolation-by-distance slope or global Wright's fixation index F_{ST}) and PLD. In contrast, D'aloia et al. (2015) observed that individual PLDs were not correlated with dispersal distance based on genetic parentage analysis. More recently, Shi et al. (2024) reported a very strong linear correlation ($R^2=0.98$) between PLD and travel distance (distance along transport trajectories), while only a moderate correlation ($R^2=0.85$) between PLD and linear distance. In this 370 study, mean orthodromic distance from release location center to settlement center (d_m) increased with increasing PLD (Fig. 7), while the overall correlation between individual dispersal distances and PLD was weak (Pearson correlation = 0.245, Spearman correlation = 0.236). This suggests that, although PLD captures broad, average trends in dispersal potential, it is not a reliable predictor of dispersal distance at the individual level. Longer PLD does not necessarily lead to a longer dispersal distance for individual larvae because larval trajectories are strongly influenced by topographic constraints on flow, and 375 oscillatory flows, such as tides and seiches.

4.3 Weibull and Generalized Gaussian 1D Dispersal Kernels

The Weibull 1D dispersal kernel is consistent with previous Lagrangian particle tracking simulations, but differs from genetic parentage analyses, in which generalized Gaussian dispersal kernel were commonly used:

$$\rho(k, d) = \exp [-(kd)^c]$$

380 where k is the scale parameter, and c is a shape parameter defining the form of the kernel. When $c = 1$, the kernel reduces to the classical exponential decay model, also referred to as the Laplacian; $c = 2$ gives the Gaussian (bell-shaped) distribution and $c = 3$ yields a Ribbens function (Almany et al., 2013; Almany et al., 2017). Notably, this formulation is not explicitly

normalized with a scale coefficient, as normalization is implicitly handled within likelihood-based connectivity models. In this kernel family, dispersal strength decreases monotonically with increasing dispersal distance, with the modal dispersal distance occurring at the source location.

385

Consistent with this property, genetic parentage analyses commonly infer kernels peaking at the natal reef (source location). For example, D'aloia et al. (2015) and Almany et al. (2017) applied a Laplacian kernel to reef fish (*Elacatinus lori*; PLD: 15 – 42 d) on the Belize Barrier Reef, and clownfish (*Amphiprion percula*; PLD: 10 – 12 d) and butterflyfish (*Chaetodon vagabundus*; PLD: 28 – 45 d) in Papua New Guinea. Hamilton et al. (2021) fitted a Ribbens dispersal kernel for *Bolbometopon muricatum* (PLD: ~ 25 d) larvae in Solomon Islands. Catalano et al. (2021) and Dedrick et al. (2021) applied generalized Gaussian kernels for *Amphiprion clarkii* (PLD: 7 – 10 d) along a 30-km Philippines coastline.

390

In contrast, Lagrangian particle-tracking studies often predict kernels with non-zero modal dispersal distances. Siegel et al. (2003) employed a Gaussian dispersal kernel to approximate the mechanisms of larval transport in turbulent coastal flows, with a modal dispersal distance of ~ 208 km for long PLDs (0 ~ 56 d). Vaz et al. (2023) used a biophysical connectivity model (Connectivity Modeling System) to study larval dispersal of *Lutjanus campechanus* in the Gulf of Mexico, predicting a modal distance of ~50 km (PLD: 26 – 30 d). Similarly, Nickols et al. (2015) found modal dispersal distances of 50–150 km using particle-tracking simulations with and without a coastal boundary layer (PLD: 2 – 30 d).

395

Consistent with these biophysical results, the best-fitting 1D dispersal kernel in the present study was a Weibull function, which predicts a non-zero modal dispersal distance (44 – 151 km) and broader dispersal, with 50% of larvae settling 110–196 km from the source. The discrepancy between Weibull and Gaussian kernels may be attributed to several factors, including but not limited to two main aspects. First, parentage analyses rely on in situ observations and typically capture only a limited number of dispersal events within specific time windows and locations, potentially missing long-distance dispersal occurring farther from the source. Second, many simulations assume passive larvae and neglect active swimming behavior. In reality, larval behaviors such as oriented swimming toward the source, may reduce dispersal distances and alter the shape of the dispersal kernel. Further investigation that integrates parentage analysis with biophysical modeling is thus required to elucidate the mechanisms underlying these contrasting dispersal patterns.

405

4.4 Connectivity Between China Sea and Japanese Sea Stocks

Whether populations from the China Sea and the Japan Sea spawning grounds belong to the same or separate stocks remains unknown; here we demonstrate that they are connected through Changjiang (CJ) spawning ground. Using genetic analyses, Yu et al. (2002) reported that the Japanese anchovy populations from spawning grounds near northeastern Taiwan, in the Pacific Ocean, and near southwestern Taiwan, in the Taiwan Strait, were indeed separate stocks. In contrast, Yu et al. (2005) and Zheng et al. (2015) found no significant genetic differentiation among populations from the Yellow Sea and East China Sea. Furthermore, marginally significant genetic structure was detected between the Bohai Sea and Japan Sea populations, as well as between the North Yellow Sea and Japan Sea population (Zhang et al., 2020a). Results from the present larval dispersal study indicate that stocks from the China Sea and the Japan Sea are dynamically connected, with the Changjiang (CJ) spawning

415



ground playing a pivotal role. Larvae originating from CJ were transported to both the northwest of Kyushu (TWC) and south of Kyushu (PS) of the Japan Sea, as well as to the central Yellow Sea, where they mix with larvae from other China Sea spawning grounds. If the CJ spawning ground were to disappear, this connectivity would likely be disrupted, potentially leading to future separation of the two stocks.

420 4.5 Limitations and Implications for Fisheries Management

Despite providing new insights into larval dispersal and connectivity of Japanese anchovy in the China Seas, several limitations should be acknowledged. First, the particle-tracking simulations assumed predominantly passive larval transport and did not explicitly incorporate active swimming behaviors (e.g., rheotaxis or directional swimming), which may influence realized dispersal distances and connectivity patterns. Second, biological processes such as growth, mortality, predation, and habitat selection were not explicitly represented; for example, larvae released from different locations will experience different water temperature, thus affect larval growth rate and travel duration. Notably, this study focused on connectivity among spawning grounds rather than between spawning and nursery grounds, as the latter remain insufficiently characterized. Further research is therefore needed to identify nursery habitats and quantify spawning–nursery connectivity.

The findings of this study have several important implications for fisheries management and conservation of Japanese anchovy. First, the dominant role of spawning location in shaping dispersal and connectivity highlights the need to prioritize the protection of key spawning grounds, particularly the Changjiang (CJ) spawning ground, which acts as a critical source connecting populations across the China Seas and the Sea of Japan. Second, the identification of the Bohai Sea, northern Yellow Sea, and southern Shandong Peninsula as major nursery areas suggests that these regions should be considered priority zones for habitat conservation and management. Third, the strong seasonal variability in dispersal patterns indicates that management strategies should account for temporal dynamics. Adaptive, season-specific management approaches may therefore improve conservation outcomes. Fourth, the relatively minor contribution of interannual variability compared to spatial factors suggests that management efforts should focus more on persistent spatial structures rather than short-term fluctuations. Finally, the quantified dispersal kernels provide a useful framework for incorporating connectivity into stock assessment and spatial management models. Integrating such metrics into fisheries management could improve predictions of recruitment dynamics, enhance the design of marine protected areas, and support ecosystem-based management strategies.

5 Conclusions

This study addresses a critical knowledge gap in quantifying larval dispersal patterns of Japanese anchovy (*Engraulis japonicus*) in the China Seas, by integrating the Lagrangian particle-tracking simulations with 1D and 2D dispersal kernels. MANOVA was performed to identify the main drivers in shaping larval dispersal patterns, including spawning ground, travel duration, spawning month and year. Larvae settled over a wide range, while were concentrated in the Bohai Sea, the northern Yellow Sea and along the southern coast of the Shandong Peninsula, with peak densities near 39°N. A Weibull 1D dispersal kernel



best described larval dispersal patten, with modal dispersal distances ranges from 44.53 – 150.56 km, identifying these regions as major nursery grounds. Among all factors examined, spawning ground was the dominant driver of dispersal and connectivity, explaining 31.1% of the variance. Settlement locations varied among spawning grounds: larvae from BHB and LZB remained within the Bohai Sea, those from ZH, YT, SDI, and HZB settled mainly in the Yellow Sea, whereas larvae from CJ dispersed more broadly to the Yellow Sea, Sea of Japan, and the northwestern Pacific, highlighting the pivotal role of CJ in linking stocks between these regions. In addition, CJ exhibited dispersal distance approximately twice those of LZB, yet with comparable spatial occupation, indicating that greater dispersal distance does not necessarily translate into broader spatial occupation. Dispersal patterns exhibited strong seasonal shifts, with enhanced eastward and northward export in spring–early summer and increased retention in late summer. Pelagic larval duration captured mean dispersal trends but was a poor predictor of individual dispersal outcomes. The relatively minor contribution of interannual variability compared to spatial factors suggests that management should focus more on persistent spatial structures rather than short-term fluctuations. Overall, these findings provide a comprehensive framework for understanding larval dispersal dynamics and offer a robust scientific basis for fisheries management and stock connectivity assessment of Japanese anchovy.

460 **Code and data availability**

Date and code are available at <https://zenodo.org/uploads/19470528> (Shi et al., 2026b).

Author contributions

WS: Conceptualization; Data Curation; Formal Analysis; Investigation; Methodology; Software; Visualization; Writing - Original Draft Preparation; Writing – Review & Editing. LB: Conceptualization; Review & Editing. SLS: Conceptualization; Reviewing & Editing. YJT: Funding Acquisition; Conceptualization; Supervision. YL: Reviewing & Editing. PS: Reviewing & Editing. ZJY: Reviewing & Editing. QWX: Data Curation; Reviewing & Editing. JCL: Supervision; Reviewing & Editing.

Competing interests

The authors declare that they have no conflict of interest.

Financial support

470 This work was supported by the National Natural Science Foundation of China (42376100) and the National Key Research and Development Program of China (2023YFD2401103).



References

- Almany, G. R., Hamilton, R. J., Bode, M., Matawai, M., Potuku, T., Saenz-Agudelo, P., Planes, S., Berumen, M. L., Rhodes, K. L., Thorrold, S. R., Russ, G. R., and Jones, G. P.: Dispersal of grouper larvae drives local resource sharing in a coral reef fishery, *Curr Biol*, 23, 626-630, 10.1016/j.cub.2013.03.006, 2013.
- Almany, G. R., Planes, S., Thorrold, S. R., Berumen, M. L., Bode, M., Saenz-Agudelo, P., Bonin, M. C., Frisch, A. J., Harrison, H. B., Messmer, V., Nanninga, G. B., Priest, M. A., Srinivasan, M., Sinclair-Taylor, T., Williamson, D. H., and Jones, G. P.: Larval fish dispersal in a coral-reef seascape, *Nat Ecol Evol*, 1, 148, 10.1038/s41559-017-0148, 2017.
- Ayata, S.-D., Lazure, P., and Thiébaud, É.: How does the connectivity between populations mediate range limits of marine invertebrates? A case study of larval dispersal between the Bay of Biscay and the English Channel (North-East Atlantic), *Progress in Oceanography*, 87, 18-36, 10.1016/j.pocean.2010.09.022, 2010.
- Botsford, Hastings, and Gaines: Dependence of sustainability on the configuration of marine reserves and larval dispersal distance, *Ecology Letters*, 4, 144-150, 10.1046/j.1461-0248.2001.00208.x, 2001.
- Botsford, L. W., White, J. W., Coffroth, M. A., Paris, C. B., Planes, S., Shearer, T. L., Thorrold, S. R., and Jones, G. P.: Connectivity and resilience of coral reef metapopulations in marine protected areas: matching empirical efforts to predictive needs, *Coral Reefs*, 28, 327-337, 10.1007/s00338-009-0466-z, 2009.
- Catalano, K. A., Dedrick, A. G., Stuart, M. R., Puritz, J. B., Montes, H. R., Jr., and Pinsky, M. L.: Quantifying dispersal variability among nearshore marine populations, *Mol Ecol*, 30, 2366-2377, 10.1111/mec.15732, 2021.
- Chaput, R., Sochala, P., Miron, P., Kourafalou, V. H., Iskandarani, M., and Kaplan, D. M.: Quantitative uncertainty estimation in biophysical models of fish larval connectivity in the Florida Keys, *ICES Journal of Marine Science*, 79, 609-632, 10.1093/icesjms/fsac021, 2022.
- Choi, J.-G., Jo, Y.-H., Moon, I.-J., Park, J., Kim, D.-W., and Lippmann, T. C.: Physical forces determine the annual bloom intensity of the giant jellyfish *Nemopilema nomurai* off the coast of Korea, *Regional Studies in Marine Science*, 24, 55-65, 10.1016/j.rsma.2018.07.003, 2018.
- Cowen, R. K. and Sponaugle, S.: Larval Dispersal and Marine Population Connectivity, *Annual Review of Marine Science*, 1, 443-466, 10.1146/annurev.marine.010908.163757, 2009.
- D'Aloia, C. C., Bogdanowicz, S. M., Francis, R. K., Majoris, J. E., Harrison, R. G., and Buston, P. M.: Patterns, causes, and consequences of marine larval dispersal, *Proc Natl Acad Sci U S A*, 112, 13940-13945, 10.1073/pnas.1513754112, 2015.
- Dedrick, A. G., Catalano, K. A., Stuart, M. R., White, J. W., Montes, H. R., Jr., and Pinsky, M. L.: Persistence of a reef fish metapopulation via network connectivity: theory and data, *Ecol Lett*, 24, 1121-1132, 10.1111/ele.13721, 2021.
- Edwards, K. P., Hare, J. A., Werner, F. E., and Seim, H.: Using 2-dimensional dispersal kernels to identify the dominant influences on larval dispersal on continental shelves, *Marine Ecology Progress Series*, 352, 77-87, 10.3354/meps07169, 2007.
- Faillietaz, R., Paris, C. B., and Irisson, J.-O.: Larval Fish Swimming Behavior Alters Dispersal Patterns From Marine Protected Areas in the North-Western Mediterranean Sea, *Frontiers in Marine Science*, 5, 10.3389/fmars.2018.00097, 2018.
- Gamoyo, M., Obura, D., and Reason, C. J. C.: Estimating Connectivity Through Larval Dispersal in the Western Indian Ocean, *Journal of Geophysical Research: Biogeosciences*, 124, 2446-2459, 10.1029/2019jg005128, 2019.
- Hamilton, R. J., Lozano-Cortés, D., Bode, M., Almany, Glenn R., Harrison, H. B., Pita, J., Saenz-Agudelo, P., Gereniu, C., Waldie, P. A., Peterson, N., Choat, J. H., and Berumen, M. L.: Larval dispersal and fishing pressure influence recruitment in a coral reef fishery, *Journal of Applied Ecology*, 58, 2924-2935, 10.1111/1365-2664.14027, 2021.
- Hao, W., Jian, S., Ruijing, W., Lei, W., and Yi'an, L.: Tidal front and the convergence of anchovy (*Engraulis japonicus*) eggs in the Yellow Sea, *Fisheries Oceanography*, 12, 434-442, 10.1046/j.1365-2419.2003.00259.x, 2003.
- Hinrichsen, H.-H., Kühn, W., Peck, M. A., and Voss, R.: The impact of physical and biological factors on the drift and spatial distribution of larval sprat: A comparison of the Baltic and North Seas, *Progress in Oceanography*, 107, 47-60, 10.1016/j.pocean.2012.05.004, 2012.
- Huggett, J., Fréon, P., Mullon, C., and Penven, P.: Modelling the transport success of anchovy *Engraulis encrasicolus* eggs and larvae in the southern Benguela: the effect of spatio-temporal spawning patterns, *Marine Ecology Progress Series*, 250, 247-262, 2003.
- Huret, M., Petitgas, P., and Woillez, M.: Dispersal kernels and their drivers captured with a hydrodynamic model and spatial indices: A case study on anchovy (*Engraulis encrasicolus*) early life stages in the Bay of Biscay, *Progress in Oceanography*, 87, 6-17, 10.1016/j.pocean.2010.09.023, 2010.



- Iseki, K. and Kiyomoto, Y.: Distribution and settling of Japanese anchovy (*Engraulis japonicus*) eggs at the spawning ground off Changjiang River in the East China Sea, *Fisheries Oceanography*, 6, 205-210, 10.1046/j.1365-2419.1997.00040.x, 1997.
- Itoh, S., Yasuda, I., Nishikawa, H., Sasaki, H., and Sasai, Y.: Transport and environmental temperature variability of eggs and larvae of the Japanese anchovy (*Engraulis japonicus*) and Japanese sardine (*Sardinops melanostictus*) in the western North Pacific estimated via numerical particle-tracking experiments, *Fisheries Oceanography*, 18, 118-133, 10.1111/j.1365-2419.2009.00501.x, 2009.
- Langsrud, Ø.: 50–50 multivariate analysis of variance for collinear responses, *The Statistician*, 51(3), 305-317, 2002.
- Lett, C., Ayata, S.-D., Huret, M., and Irisson, J.-O.: Biophysical modelling to investigate the effects of climate change on marine population dispersal and connectivity, *Progress in Oceanography*, 87, 106-113, 10.1016/j.pocean.2010.09.005, 2010.
- 525 Lett, C., Penven, P., Ayón, P., and Fréon, P.: Enrichment, concentration and retention processes in relation to anchovy (*Engraulis ringens*) eggs and larvae distributions in the northern Humboldt upwelling ecosystem, *Journal of Marine Systems*, 64, 189-200, 10.1016/j.jmarsys.2006.03.012, 2007.
- Lett, C., Roy, C., Lévasseur, A., Van Der Lingen, C. D., and Mullon, C.: Simulation and quantification of enrichment and retention processes in the southern Benguela upwelling ecosystem, *Fisheries Oceanography*, 15, 363-372, 10.1111/j.1365-2419.2005.00392.x, 2006.
- 530 Liang, S. and Sun, Z.: Typical Seasonal Circulation in the Bohai Sea, ISOPE International Ocean and Polar Engineering Conference, 2003.
- Masuda, R.: Ontogeny of swimming speed, schooling behaviour and jellyfish avoidance by Japanese anchovy *Engraulis japonicus*, *J Fish Biol*, 78, 1323-1335, 10.1111/j.1095-8649.2011.02936.x, 2011.
- 540 Nathan, R.: Long-distance dispersal of plants, *Science*, 313, 2008.
- Nathan, R., Schurr, F. M., Spiegel, O., Steinitz, O., Trakhtenbrot, A., and Tsoar, A.: Mechanisms of long-distance seed dispersal, *Trends Ecol Evol*, 23, 638-647, 10.1016/j.tree.2008.08.003, 2008.
- Nickols, K. J., White, J. W., Largier, J. L., and Gaylord, B.: Marine population connectivity: reconciling large-scale dispersal and high self-retention, *Am Nat*, 185, 196-211, 10.1086/679503, 2015.
- 545 Paris, C. B. and Cowen, R. K.: Direct evidence of a biophysical retention mechanism for coral reef fish larvae, *Limnology and Oceanography*, 49, 1964-1979, 10.4319/lo.2004.49.6.1964, 2004.
- Paris, C. B., Chérubin, L. M., and Cowen, R. K.: Surfing, spinning, or diving from reef to reef: effects on population connectivity, *Marine Ecology Progress Series*, 347, 285-300, 10.3354/meps06985, 2007.
- Paris, C. B., Helgers, J., van Sebille, E., and Srinivasan, A.: Connectivity Modeling System: A probabilistic modeling tool for the multi-scale tracking of biotic and abiotic variability in the ocean, *Environmental Modelling & Software*, 42, 47-54, 10.1016/j.envsoft.2012.12.006, 2013.
- 550 Puckett, B. J., Eggleston, D. B., Kerr, P. C., and Luettich, R. A.: Larval dispersal and population connectivity among a network of marine reserves, *Fisheries Oceanography*, 23, 342-361, 10.1111/fog.12067, 2014.
- Sato, M., Honda, K., Nakamura, Y., Bernardo, L. P. C., Bolisay, K. O., Yamamoto, T., Herrera, E. C., Nakajima, Y., Lian, C., Uy, W. H., Fortes, M. D., Nadaoka, K., and Nakaoka, M.: Hydrodynamics rather than type of coastline shapes self-recruitment in anemonefishes, *Limnology and Oceanography*, 69, 10.1002/lno.12399, 2023.
- 555 Selkoe, K. A. and Toonen, R. J.: Marine connectivity: a new look at pelagic larval duration and genetic metrics of dispersal, *Marine Ecology Progress Series*, 436, 291-305, 10.3354/meps09238, 2011.
- Shanks, A., L., Grantham, B. A., and Carr, M. H.: Propagule dispersal distance and the size and spacing of marine reserves, *Ecological Applications*, 13 (1), 2003.
- 560 Shanks, A. L.: Pelagic larval duration and dispersal distance revisited, *Biol. Bull.*, 216, 373-385, 2009.
- Shi, W., Boegman, L., Ackerman, J. D., Shan, S., and Zhao, Y.: Computation of fish larvae self-recruitment in using forward- and backward-in-time particle tracking in a Lagrangian model (SWIM-v2.0) of the simulated circulation of Lake Erie (AEM3D-v1.1.2), *Geoscientific Model Development*, 19, 1213-1228, 10.5194/gmd-19-1213-2026, 2026a.
- 565 Shi, W., Shao, D., Gualtieri, C., Purnama, A., and Cui, B.: Modelling long-distance floating seed dispersal in salt marsh tidal channels, *Ecohydrology*, 13, 10.1002/eco.2157, 2019.
- Shi, W., Boegman, L., Shan, S., Zhao, Y., Ackerman, J. D., Amidon, Z., Jabbari, A., and Roseman, E.: A Larval “Recruitment Kernel” to Predict Hatching Locations and Quantify Recruitment Patterns, *Water Resources Research*, 60, 10.1029/2023wr036099, 2024.



- 570 Shi, W., Boegman, L., Shan, S., Tian, Y., Liu, Y., Sun, P., Ye, Z., Xing, Q., and Li, J.: Data for for manuscript: Quantifying Patterns and Drivers of Larval Dispersal in Japanese Anchovy (*Engraulis japonicus*) in the China Seas [dataset], 2026b. Siegel, D. A., Kinlan, B. P., Gaylord, B., and Gaines, S. D.: Lagrangian descriptions of marine larval dispersion, *Marine Ecology Progress Series*, 260, 83-96, 10.3354/meps260083, 2003.
- 575 Sponaugle, S., Paris, C., Walter, K. D., Kourafalou, V., and D'Alessandro, E.: Observed and modeled larval settlement of a reef fish to the Florida Keys, *Marine Ecology Progress Series*, 453, 201-212, 10.3354/meps09641, 2012. Takeshige, A., Miyake, Y., Nakata, H., Kitagawa, T., and Kimura, S.: Simulation of the impact of climate change on the egg and larval transport of Japanese anchovy (*Engraulis japonicus*) off Kyushu Island, the western coast of Japan, *Fisheries Oceanography*, 24, 445-462, 10.1111/fog.12121, 2015.
- 580 Tu, C. Y., Tseng, Y. H., Chiu, T. S., Shen, M. L., and Hsieh, C. H.: Using coupled fish behavior–hydrodynamic model to investigate spawning migration of Japanese anchovy, *Engraulis japonicus*, from the East China Sea to Taiwan, *Fisheries Oceanography*, 21, 255-268, 10.1111/j.1365-2419.2012.00619.x, 2012. Vaz, A. C., Karnauskas, M., Smith, M., Denson, L. S., Paris, C. B., Le Hénaff, M., and Siegfried, K.: Red Snapper connectivity in the Gulf of Mexico, *Marine and Coastal Fisheries*, 15, 10.1002/mcf2.10275, 2023.
- 585 Willis, J.: Modelling swimming aquatic animals in hydrodynamic models, *Ecological Modelling*, 222, 3869-3887, 10.1016/j.ecolmodel.2011.10.004, 2011. Woillez, M., Rivoirard, J., and Petitgas, P.: Notes on survey-based spatial indicators for monitoring fish populations, *Aquatic Living Resources*, 22, 155-164, 10.1051/alr/2009017, 2009.
- Wood, S., Paris, C. B., Ridgwell, A., and Hendy, E. J.: Modelling dispersal and connectivity of broadcast spawning corals at the global scale, *Global Ecology and Biogeography*, 23, 1-11, 10.1111/geb.12101, 2013.
- 590 Xing, Q., Yu, H., Yu, H., Sun, P., Liu, Y., Ye, Z., Li, J., and Tian, Y.: A comprehensive model-based index for identification of larval retention areas: A case study for Japanese anchovy *Engraulis japonicus* in the Yellow Sea, *Ecological Indicators*, 116, 10.1016/j.ecolind.2020.106479, 2020. Xing, Q., Yu, H., Ito, S.-i., Ma, S., Yu, H., Wang, H., Tian, Y., Sun, P., Liu, Y., Li, J., and Ye, Z.: Using a larval growth index to detect the environment-recruitment relationships and its linkage with basin-scale climate variability: A case study for Japanese anchovy (*Engraulis japonicus*) in the Yellow Sea, *Ecological Indicators*, 122, 10.1016/j.ecolind.2020.107301, 2021.
- 595 Ye, M. Z. and Zhang, Z.: The distribution and behaviour of *Engraulis japonicus* Temminck and schlegel and its detection in the north China Seas (Hwang-hai and Po-hai), *Journal of Fisheries of China*, 2, 27-34, 1965. Yu, H., Yu, H., Ito, S.-i., Tian, Y., Wang, H., Liu, Y., Xing, Q., Bakun, A., and Kelly, R. M.: Potential environmental drivers of Japanese anchovy (*Engraulis japonicus*) recruitment in the Yellow Sea, *Journal of Marine Systems*, 212, 10.1016/j.jmarsys.2020.103431, 2020a.
- 600 Yu, H. T., Lee, Y. J., Huang, S. W., and Chiu, T. S.: Genetic analysis of the populations of Japanese anchovy (*Engraulidae*: *Engraulis japonicus*) using microsatellite DNA, *Mar Biotechnol (NY)*, 4, 471-479, 10.1007/s10126-002-0035-8, 2002. Yu, J. Z., Zhang, Y. W., Bian, X. D., Chen, Y. L., and Zhang, X. Q.: Key impact factor identification and future distribution prediction of the anchovy spawning ground in the Bohai Sea, *China Environmental Science*, 40(5), 2214-2221, 10.19674/j.cnki.issn1000-6923.2020.0253, 2020b.
- 605 Yu, Z. N., Kong, X. Y., Guo, T. H., Jiang, Y. Y., Zhuang, Z. M., and Jin, X. S.: Mitochondrial DNA sequence variation of Japanese anchovy *Engraulis japonicus* from the Yellow Sea and East China Sea, *Fisheries Science*, 71, 299-307, 2005. Zenitani, H. and Kimura, R.: Elemental analysis of otoliths of Japanese anchovy: trial to discriminate between Seto Inland Sea and Pacific otck, *Fisheries Science*, 73, 2007.
- 610 Zhang, B.-D., Li, Y.-L., Xue, D.-X., and Liu, J.-X.: Population Genomics Reveals Shallow Genetic Structure in a Connected and Ecologically Important Fish From the Northwestern Pacific Ocean, *Frontiers in Marine Science*, 7, 10.3389/fmars.2020.00374, 2020a. Zhang, W., Yu, H., Ye, Z., Tian, Y., Liu, Y., Li, J., Xing, Q., and Jiang, Y.: Spawning strategy of Japanese anchovy *Engraulis japonicus* in the coastal Yellow Sea: Choice and dynamics, *Fisheries Oceanography*, 30, 366-381, 10.1111/fog.12523, 2020b.
- 615 Zhao, X., Hamre, J., Li, F., Jin, X., and Tang, Q.: Recruitment, sustainable yield and possible ecological consequences of the sharp decline of the anchovy (*Engraulis japonicus*) stock in the Yellow Sea in the 1990s, *Fisheries Oceanography*, 12, 495-501, 10.1046/j.1365-2419.2003.00262.x, 2003. Zhao, X. Y.: Population dynamic characteristics and sustainable utilization of the anchovy stock in the Yellow Sea, Ocean University of China, Qingdao, 2006.



- 620 Zhao, Y., Jones, M. L., Shuter, B. J., and Roseman, E. F.: A biophysical model of Lake Erie walleye (*Sander vitreus*) explains interannual variations in recruitment, *Canadian Journal of Fisheries and Aquatic Sciences*, 66, 114-125, 10.1139/f08-188, 2009.
- Zheng, W., Zou, L., and Han, Z.: Genetic analysis of the populations of Japanese anchovy *Engraulis japonicus* from the Yellow Sea and East China Sea based on mitochondrial cytochrome b sequence, *Biochemical Systematics and Ecology*, 58, 169-177, 10.1016/j.bse.2014.12.007, 2015.

625